Inhomogeneous kinetic effects related to intermittent magnetic discontinuities

A. Greco, F. Valentini, and S. Servidio

Dipartimento di Fisica, Università della Calabria, I-87036 Cosenza, Italy

W. H. Matthaeus

Bartol Research Institute and Department of Physics and Astronomy, University of Delaware, Newark, Delaware 19716, USA

A connection between kinetic processes and two-dimensional intermittent plasma turbulence is observed using direct numerical simulations of a hybrid Vlasov-Maxwell model, in which the Vlasov equation is solved for protons, while the electrons are described as a massless fluid. During the development of turbulence, the proton distribution functions depart from the typical configuration of local thermodynamic equilibrium, displaying *statistically* significant non-Maxwellian features. In particular, temperature anisotropy and distortions are concentrated near coherent structures, generated as the result of the turbulent cascade, such as current sheets, which are nonuniformly distributed in space. Here, the partial variance of increments (PVI) method has been employed to identify high magnetic stress regions within a two-dimensional turbulent pattern. A quantitative association between non-Maxwellian features and coherent structures is established.

PACS number(s): 96.50.−e

I. INTRODUCTION

The solar wind is a weakly collisional ionized gas generally observed in a turbulent state [1,2]. At magnetohydrodynamics (MHD) scales, energy spectra in the interplanetary and interstellar gas are frequently reminiscent of the Kolmogorov inertial range [3] for fluid turbulence. The cascade from the energy injection scales, through the inertial range, and toward the dissipation scales may be described adequately by MHD—itself an incomplete subject. However at smaller, kinetic scales there are new physical ingredients, as evidenced by numerous characteristic spatial and temporal scales (the ion (electron) inertial length and Larmor radius and the ion (electron) cyclotron frequencies). In recent years, there has been substantial interest in identifying the physical mechanisms operating at these kinetic scales, and understanding how these act to provide dissipation and particle heating [4–6].

Great effort has been directed to the analysis of the observational data from the new generation of spacecraft that provide information about previously inaccessible kinetic regimes. Moreover, continual increase in computational resources has enabled sophisticated kinetic numerical simulations that describe plasma dynamics at these scales. These modern numerical tools provide indispensable support for interpretation of direct measurements of kinetic properties in the solar wind.

The turbulent solar wind is characterized by broad band electromagnetic fluctuations, and sharp magnetic shears (or magnetic discontinuities). The question arises from the perspective of turbulence theory: are these discontinuities associated with the dynamical turbulence phenomenon of intermittency? In hydrodynamics, coherent structures are associated with intermittency of dissipation. In MHD, strong, small scale electric current structures have been identified as characteristic coherent structures, where Ohmic dissipation is concentrated [7–9]. However, the extension of these ideas to solar wind plasma physics has been slow in development. For example, an alternative might be that coherent structures are remnants of coronal boundaries [10], that interplanetary turbulence is essentially coherent, and therefore the analogies

between solar wind and hydrodynamic turbulence do not extend beyond the level of second order statistics and the energy spectrum. Convincing demonstration that coherent structures are associated with kinetic scale dissipation that terminate the cascade would support the hypothesis of intermittent turbulence and the relevance of higher order statistics in astrophysical plasma turbulence.

Solar wind discontinuities are rapid changes in properties of the plasma and magnetic field [11–13]. Early surveys identified the majority of these as rotational discontinuities (Alfvén waves), but more modern surveys identify most of them as tangential discontinuities (plasma boundaries). The time interval between the passages of consecutive strong (large angle) discontinuities varies from seconds to hours. Thicknesses of strong discontinuities vary from 10^5 km down to 10^2 km, or even smaller. The smaller of these characteristic lengths is comparable with both the ion Larmor radius and the ion skin depth [13]. Recent studies of inertial range discontinuities in the solar wind [14,15] show that their statistical distribution and waiting time distribution are very similar to distributions obtained from simulations of MHD and Hall MHD turbulence. Discontinuities at still smaller scales would be associated with coherent structures at ion and electron kinetic scales, where the inertial range terminates [16,17].

Recent works [18,19], using Wind spacecraft data in the solar wind at 1 AU, show that kinetic signatures, such as plasma heating and temperature anisotropy, are statistically associated with coherent magnetic structures (discontinuities or current sheets). Since the characteristic thickness of these non-Gaussian structures is on the order of the Larmor radius, a kinetic approach to the study of magnetic discontinuities is needed. Analysis [20] based on numerical solution of the hybrid Vlasov-Maxwell (HVM) equations [21] suggests that, in turbulence, kinetic effects such as patches of high temperature anisotropy are generated near concentrations of electric current density. Both observational and numerical analyses support the viewpoint that kinetic effects in plasmas are strongly inhomogeneous—a property related to the intermittent character of the magnetic field.

In the present work we perform a statistical analysis to further quantify the association between distinctive kinetic signatures and intermittent current sheets in a 2D-3V (two dimensions in physical space and three in velocity space) model of plasma turbulence. Using data sets from HVM self-consistent simulations [20], we investigate the link between magnetic discontinuities and the production of kinetic effects such as temperature anisotropy. Adopting 1D spacecraftlike measurements through the turbulent medium, and the partial variance of increments (PVI) method [14] for identifying discontinuities, we establish a link between the solar wind discontinuities and inhomogeneous proton kinetic effects. Kinetic features are quantified by measuring the temperature anisotropy with respect to the local magnetic field, and also employing a measure of the strength of local non-Maxwellian activity. Potential implications for the problem of turbulent reconnection are also discussed, with applications that span from astrophysical to laboratory plasmas.

The organization of the paper is as follows. In Sec. II the numerical simulations together with the analysis technique are presented. The results of our analysis will be shown in Sec. III. Discussion and conclusions will be given in Sec. IV.

II. ANALYSIS

The numerical HVM code [20–22] describes the turbulent dynamics of a magnetized plasma. In this model, the Vlasov equation for the proton distribution function f is self-consistently coupled to the Maxwell equations for the electric and magnetic fields. The electrons are treated as a massless isothermal fluid and a generalized Ohm law for the electric field is evaluated at each time step. (See Ref. [21] for more details about the HVM model and the numerical algorithm.) The assumption of quasineutrality is adopted. The macroscopic proton quantities at each point in physical space, such as particle density, bulk velocity, current density, and temperatures, can be computed through a direct integration in velocity space.

Here, we analyze the numerical results of a 2D-3V HVM simulation (Run II in Ref. [20]), of decaying turbulence. The conditions are chosen to be similar to typical conditions of the solar-wind environment. The plasma dynamics is described in a double periodic (x, y) Cartesian domain perpendicular to a background constant magnetic field $\mathbf{B}_0 = B_0\mathbf{e}_z$. The two-dimensional spatial domain is discretized by 512^2 grid points, while the three-dimensional velocity domain is represented by 51^3 grid points. The box length in physical space is $L = 2\pi \times 20d_p$ in each spatial direction, where d_p is the proton skin depth. The limits of the velocity domain are fixed at $v_{\max} = \pm 5v_{\text{thp}}$ in each velocity direction, with v_{thp} the proton thermal speed. In velocity space the proton distribution function is set equal to zero at $|v| > v_{\max}$. We point out that electron inertia terms, proportional to the squared electron skin depth, are small, but cannot be adequately described with the resolution of this HVM simulation. Therefore, these terms are ignored in our analysis. The proton plasma β, the ratio between kinetic and magnetic pressure, is set $\beta_p = 2v_{\text{thp}}^2/V_A^2 = 2$, where V_A is the Alfvén speed. An isothermal equation of state for the electron pressure is employed, and the electron to
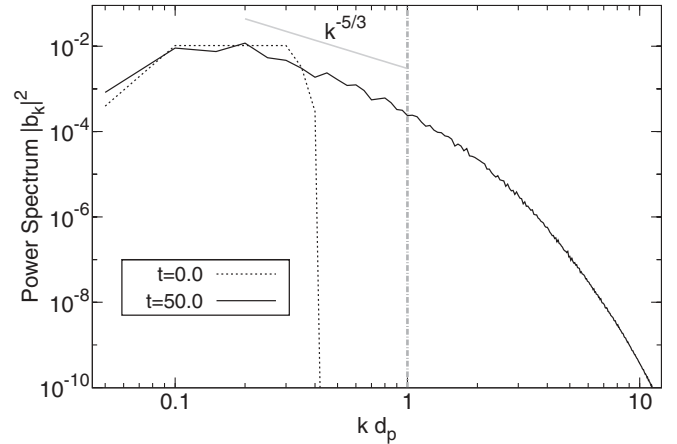
FIG. 1. Power spectra of magnetic field at $\tau = 0$ (dotted line) and $\tau = 50$ Ω_{cp}^{-1} (solid line). The Kolmogorov expectation $k^{-5/3}$ (grey solid line) is reported as a reference, while the vertical dot-dashed line represents the proton skin depth wave number.

proton temperature ratio is $T_e/T_p = 1$. The initial equilibrium, in which the protons have uniform density and a Maxwellian distribution of velocities, is perturbed by a 2D spectrum of Fourier modes, imposed for both the proton fluid velocity and the magnetic field. Energy is initialized, with random phases, in the range of wave numbers $2 \leqslant m \leqslant 6$, where the associate wave vector is $k = 2\pi m/L$. The initial magnetic and velocity perturbations have rms values such that $\delta B/B_0 = \delta v/V_A \simeq 1/3$. Tests on the total energy and entropy conservation, that measure reliability of numerical results coming from hybrid Vlasov-Maxwell simulations, show variations of 0.06% and 0.01%, respectively. More details about the setup of the numerical simulations can be found in Refs. [20,22].

We performed our analysis at a fixed instant of time $\tau = 50$ Ω_{cp}^{-1} (Ω_{cp} is the proton gyro frequency), when the maximum level of turbulent activity is reached. At this time, the solutions show the appearance of coherent structures, such as vortices (magnetic islands) and current sheets. Accordingly, the out-of-plane current density j_z becomes very intense, a clear signature of the intermittent character of the magnetic field. To characterize the turbulence in a familiar way, we compute the power spectra of the magnetic field **b** as shown in Fig. 1. Spectra reveal several features commonly observed in space plasmas. Indeed, at small scales, comparable or smaller than d_p, the spectra become steeper, due mainly to the presence of kinetic effects [1,5,6]. We note that there is some apparent similarity between the spectrum in Fig. 1 and some observations; we hesitate to claim any close correspondence, in view of the limitations of the present computations, as well as the intrinsic variability of solar wind spectra both in inertial and kinetic ranges (see, e.g., [23]).

A useful and simple way to systematically identify regions of high magnetic stress and coherent structures is based on statistics of the magnetic field increment vector $\Delta\mathbf{b}(s,\Delta s) = \mathbf{b}(s + \Delta s) - \mathbf{b}(s)$. This quantity can be readily calculated along a 1D path s within the simulation box, with a spatial separation or lag Δs. This emulates spacecraft measurements. Employing only the sequence of magnetic increments, we
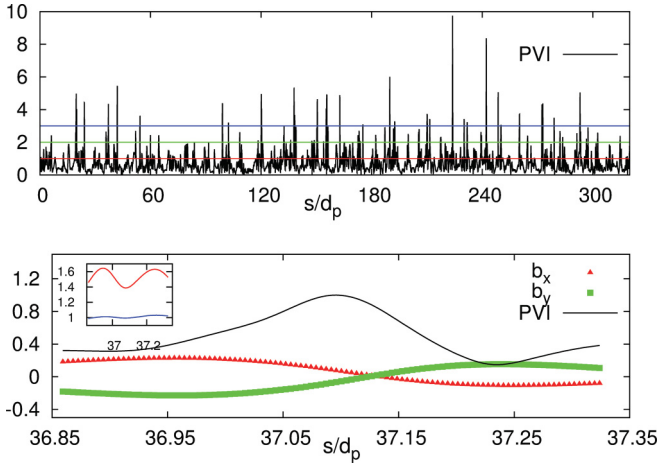
FIG. 2. (Color online) Top: PVI series obtained from simulation from Eq. (1), by sampling along the trajectory s normalized to the proton skin depth d_p. The thresholds $\theta = 1,2,3$ are also shown. Bottom: Example of discontinuities selected by the PVI method. The two components of the magnetic field vector are displayed along with the PVI signal normalized to its peak value (4.5). The inset shows the functions ϵ (%) (top red line) and A (bottom blue line) (see text for their definition) along the trajectory s.

compute the normalized magnitude

$$\Im = \frac{|\Delta\mathbf{b}|}{\sqrt{\langle|\Delta\mathbf{b}|^2\rangle}} \qquad (1)$$

where $\langle\bullet\rangle$ denotes a spatial average over the total length of the data set. The above quantity has been called the *partial variance of increments* (PVI) [14] and the method abbreviated as the PVI method. It is related to other measures of coherent structures, such as phase coherence index [24], local intermittency measure (LIM) [25], and related wavelet-based techniques for identification of coherent structures [26]. Some of these have in common that some condition (threshold) is formulated that selects parts of a data sample that are contributing to non-Gaussian statistics and therefore intermittency. The performance of the PVI in identification of discontinuities has been shown to be comparable to standard methods [12], in both MHD simulations and solar wind observations [14,15].

We expect that strong current sheets will be found over a broad range of scales extending from inertial range at least down to the proton kinetic scales. For this simulation we choose a small scale lag, $\Delta s \simeq 0.25 d_p$. A sample of the PVI measure $\Im$ along a diagonal path s, that crosses the simulation box several times [14], is shown in the top panel of Fig. 2. Here s is normalized to the proton skin depth d_p. The spatial history of $\Im$ is evidently bursty, suggesting the presence of sharp gradients and localized coherent structures in the magnetic field, that represent the spatial intermittency of turbulence. Events such as magnetic discontinuities and regions of high magnetic stress are selected by imposing a threshold on the $\Im$ series, leading to a hierarchy of coherent structures intensities. Indeed, higher and higher values of this threshold correspond to an increase likelihood of finding non-Gaussian inhomogeneous structures. An example of these events is also shown in Fig. 2, where the two in-plane components of the magnetic field are displayed along with PVI signal.

III. RESULTS

We examine local kinetic effects associated with inhomogeneous behavior of the magnetic field. In a previous work, Ref. [20] suggested that the temperature anisotropy in a turbulent cascade is concentrated in sheetlike magnetic structures (of typical size of few d_p's). Anisotropy is low inside magnetic islands while it is high in between them. These are regions of strong magnetic stress. To further investigate these kinetic effects, and how they can be quantified from single spacecraftlike measurement, here we perform a detailed inspection of the proton distribution function in 2D simulations.

To first characterize non-Maxwellian features, we compute the proton temperature anisotropy $A = T_\perp / T_\parallel$, defined as the ratio between the perpendicular and the parallel temperature with respect to the local magnetic field. The initial condition is set up to have isotropic temperature at $t = 0$. Nevertheless, during the development of turbulence the temperatures do not remain isotropic everywhere, but rather present local enhancements and depressions nearby the regions of high magnetic stress [20].

A complementary estimate of non-Maxwellian plasma behavior is given by a measure of the deviation of the proton distribution from an equivalent Maxwellian. In particular we define

$$\epsilon(x,y) = \frac{1}{n}\sqrt{\int (f-g)^2 d^3v} \qquad (2)$$

where g is the associated equivalent Maxwellian distribution computed from the parameters of f. The explicit form of the latter is

$$g = C \exp\left[-\frac{1}{2T_{\text{iso}}}\sum_j (v_j - \langle v_j\rangle)^2\right], \qquad (3)$$

where $\langle v_j\rangle$ is computed from $\langle\mathbf{v}\rangle = \frac{1}{n}\int \mathbf{v} f d^3v$, the density $n(x,y) = \int f(x,y,\mathbf{v})d^3v$, and $T_{\text{iso}} = \frac{1}{3n}\int\sum_{j=x,y,z}(v_j - \langle v_j\rangle)^2 f d^3v$, for a normalization constant C that depends on n. Note that $f(x,y,\mathbf{v},t=0) = g(x,y,\mathbf{v},t=0)$.

From the spacecraftlike sampling of the magnetic field data along a linear trajectory, discontinuities can be identified by the PVI method with a selected threshold. Figure 3 illustrates the location of discontinuities along the path s, together with shaded contours of ϵ defined in Eq. (2), and in-plane magnetic field lines. The figure reveals the association between sheetlike regions of non-Maxwellian behavior and location of magnetic discontinuities or current sheets (red open squares).

In order to further investigate these strong local kinetic effects, we compute the skewness of f, defined by

$$S_i = \frac{1}{n}\int (v_i - \langle v_i\rangle)|\mathbf{v} - \langle\mathbf{v}\rangle|^2 f d^3v, \qquad (4)$$

where $i = x, y, z$, and the kurtosis as

$$\chi_i = \frac{\frac{1}{n}\int (v_i - \langle v_i\rangle)^4 f d^3v}{\left[\frac{1}{n}\int (v_i - \langle v_i\rangle)^2 f d^3v\right]^2}. \qquad (5)$$
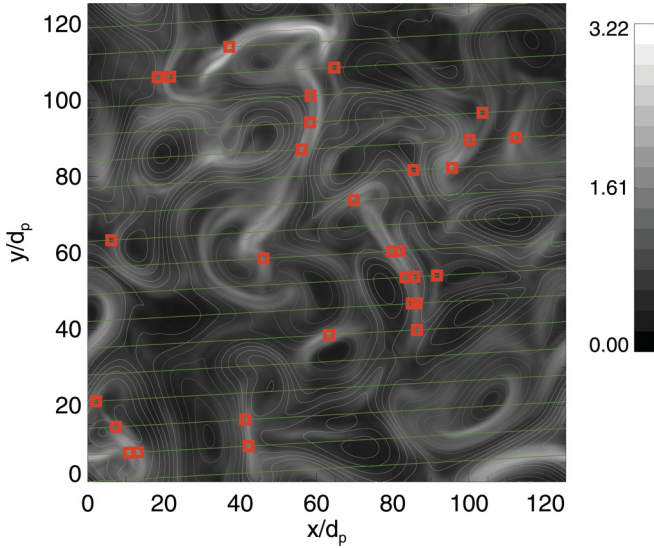
FIG. 3. (Color online) Shaded contours of the function $\epsilon(x,y)$ (in %), defined by Eq. (2), together with the magnetic flux a_z (grey and white isolines). The one-dimensional (periodic) path s is also shown (green solid line). On the same plot, the discontinuities identified by PVI technique with threshold $\theta = 3$ (red open squares) are represented. Regions of high kinetic effects are mostly concentrated near magnetic discontinuities.

Equations (4) and (5) represent the third and the fourth moment of the distribution function respectively, and note that the vectors are in physical space.

An overview of the kinetic processes that locally develop in turbulence is shown in Fig 4. In the vicinity of a PVI event, we represent ϵ, the anisotropy A, the skewness $|\mathbf{S}|$,
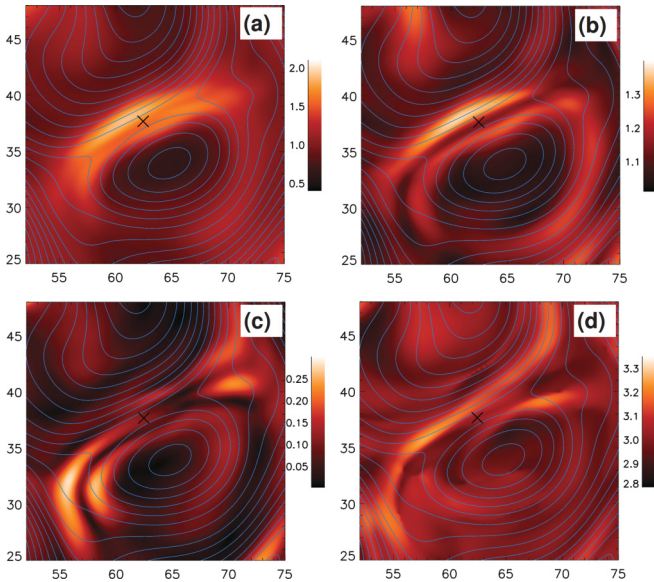
FIG. 4. (Color online) Color contours of several quantities in the vicinity of a PVI event: (a) ϵ (in %) with the in-plane magnetic field lines (blue lines). (b) Anisotropy A (c) heat flux $|\mathbf{S}|$, evaluated as the third order moment of the proton distribution function (d) Kurtosis χ_i, evaluated as the fourth order moment of the proton distribution function. The position of a PVI peak is depicted as a black cross in all panels. Note that only a portion of the box is shown.

and the kurtosis χ_i in a portion of the simulation box. Apparently, nearby these strongly active regions, anisotropy appears in sheetlike structures. Upstream of these regions a strong heat flux is present. Patterns of χ_i are localized in narrow layers in between magnetic vortices, where it reveals strong variations from Maxwellian ($\chi_i = 3$). It is clear from the figure that, when kinetic effects come into play, the distribution function f departs from the reference Maxwellian g in concentrated regions of space. The non-Maxwellian features include temperature anisotropy, nonzero skewness (heat flux), or high (low) kurtosis.

This has an important consequence for the dynamics of plasma turbulence, revealing that these kinetic responses—anisotropy, kurtosis, and heat flux—are strongly modulated by local magnetic field structure. The combination of the PVI technique along with direct measurement of non-Maxwellian features shows a strong association of discontinuities and non-Maxwellian features of kinetic origin.

To gain further insight regarding the relationship between discontinuities and kinetic effects, the probability density functions (PDFs) of ϵ have been evaluated, as well as the PDFs of the proton distribution function anisotropy $A = T_\perp / T_{||}$.
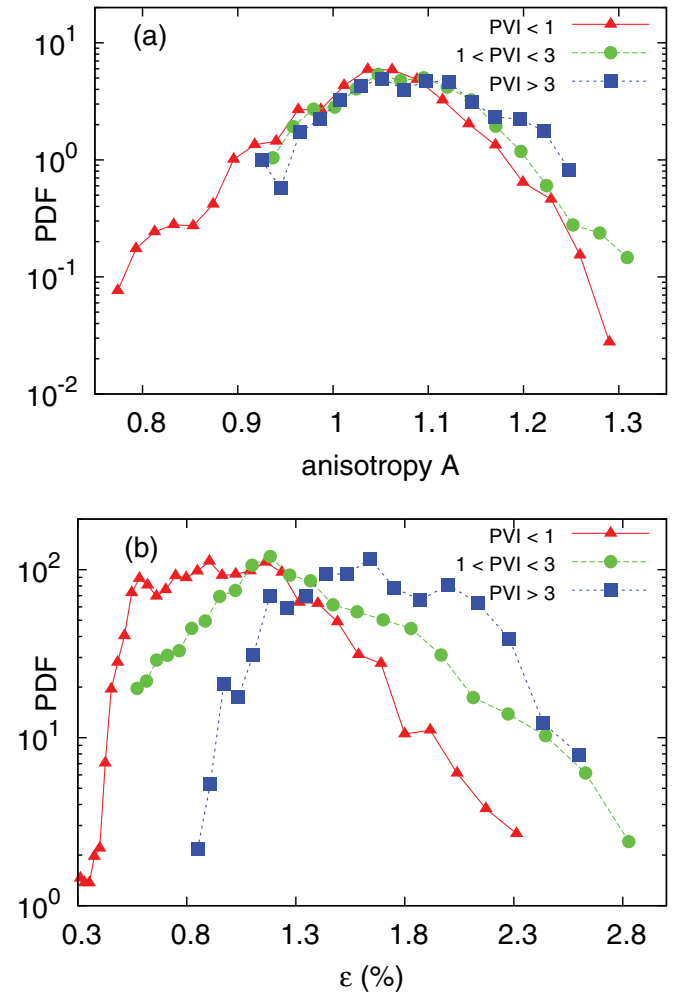
FIG. 5. (Color online) PDFs of the anisotropy A (a) and function ϵ (in %) (b). Each PDF is associated with a range of PVI.

TABLE I. PVI dependence of the average values of anisotropy A and ϵ (in %).

$\Im$	$\langle A \rangle$	$\langle \epsilon \rangle$
$\Im < 1$	1.02	1.02
$1 < \Im < 3$	1.04	1.28
$\Im > 3$	1.056	1.60

Since an association of discontinuities and kinetic quantities such as ϵ and A has been suggested above, it is useful to condition the subsequent analyses on PVI values: $\Im < 1$ corresponds to low value fluctuations (increments), $1 < \Im < 3$ removes low value fluctuations and retains the non-Gaussian structures, and $\Im > 3$ contains only most highly inhomogeneous structures including current sheets [27]. Conditional sampling methods employing the PVI method have been applied previously in solar wind observational studies [28].

Figures 5(a) and 5(b) show the PDFs of the variables A and ϵ conditioned on PVI. These plots suggest that the largest and most important distortions of the proton distribution function occur in the immediate vicinity of discontinuities ($\Im > 3$) and not in the smoothest regions ($\Im < 1$). The two panels provide strong evidence that coherent structures are connected to enhanced distortions of the distribution function, but also suggest that there exists a hierarchy of current sheet intensities, where the most intense are associated with the most nonhomogeneous kinetic effects, as recently shown in solar wind [18,19].

In Ref. [20] it was pointed out that the strongest distortions of the proton distribution function are near the peaks of density current j_z. This means that they occur at a certain distance from PVI events, as shown in the inset of Fig. 2. Here, the 1D sampling of the anisotropy A and of the function ϵ across the magnetic discontinuity are shown, revealing the their peaks are far away from the peak of the PVI signal. To take this into account, we average A and ϵ on a certain distance from PVI events that exceed a threshold value θ [19]. This distance is about $\pm 1.2 d_p \sim 0.2\lambda_C$, where λ_C is the correlation scale of the magnetic turbulence.

Table I quantifies this PVI dependence of the average quantities. It is clear that plasma with the greatest portion of intense coherent structures ($\Im > 3$) has the largest average deviation from a local Maxwellian and highest most probable anisotropy. It is noteworthy that the changes in the averages are not large, as the data are broadly distributed.

IV. DISCUSSION AND CONCLUSION

Recent results in solar wind observations have revealed the importance of fine spatial scales and kinetic effects that may be associated with them. In turn, simulations have helped to clarify and interpret these connections. It seems increasingly clear that significant kinetic effects including heating have strong association with coherent structures and with turbulence cascade that produce intermittency. Various techniques including MHD, Hall MHD, and electromagnetic particle-in-cell (PIC) simulations have been employed in these studies. Here we employ Vlasov hybrid simulations as a complementary methodology. This approach has the advantage that the full collisionless kinetic behavior of protons is represented, however, without the discretization and counting statistics issues that enter the PIC approach. This advantage is of specific relevance to the present study of the association between non-Maxwellian features and the coherent structures identified by the PVI method. Obviously, this approach presents some limitations. For example, electron inertia terms, proportional to the squared electron skin depth, are not described with this HVM simulation, and with the currently employed resolutions, could not be well described. With the above restrictions we cannot reproduce exactly solar wind observations [6], but we can properly describe the kinetic physics at scales on the order of the Larmor radius (or proton skin depth).

The PVI-threshold method is known to perform well to find non-Gaussian tails and coherent structures, many of which are current sheets, and at higher thresholds, reconnection sites [29]. With the exception of the last point, the earlier works have been kinematic in nature. This study has shown a new direction for PVI methods that is helping us to understand dynamical processes, including dissipation and heating [18,19]. Indeed, this association, which had been previously suggested [29], has been confirmed in the present study. Non-Maxwellian features at the level of a few percent [measured by Eq. (2)] are strongly associated with PVI thresholds when analyzed using conditional probability distributions. In particular, stronger temperature anisotropy $A = T_\perp / T_\parallel$ is observed near high PVI events, which are strongly associated with coherent current structures. For values of $\beta_p \sim 1$ as used in the present simulation, the proton anisotropy A gets up to ~ 1.3, which is close to what is observed on average in the solar wind [19].

It is not so clear if this would be as readily established using PIC methods due to counting statistics, although a visual association of temperature anisotropy and sheetlike structures was reported in very high resolution PIC simulations by Ref. [17]. In any case the Vlasov approach, with direct representation of the distribution function, provides a robust approach that may have advantages in examination of detailed properties of the proton distribution function.

The stronger observed temperature anisotropies seen here near high PVI current structures are also compatible with recent solar wind observational studies. For example, computation of the distribution of proton temperatures conditioned on PVI threshold using solar wind spacecraft data reveals that higher PVI samples and therefore coherent magnetic structures are hotter [18,28]. More detailed study reveals that extremes of proton temperature anisotropy are associated with higher average PVI [19]. It is clear that the association of high PVI structures with proton kinetic effects can be established in both cases. However there are important differences. The present simulations and others [17] are limited in size so that available increment spatial lags are smaller than those probed by solar wind plasma data. Simulation lags are typically of the order of the ion inertial scale d_i, while readily available plasma data (say, 96 sec) are sensitive to much large scales ($\sim 100 d_i$).

Moreover, values of plasma β and turbulence level are more variable in the solar wind than in this simulation. Consequently, while the simulation and observational conclusions are similar, they must be regarded at present as complementary rather than

equivalent, due to differences in accessible parameters in the two cases.

The present results add to accumulating evidence that cascade, nonlinearity, and associated intermittency are important in establishing observed kinetic plasma properties in the solar atmosphere, and perhaps more broadly in astrophysical plasmas. The case for this will be further tested as simulations attain greater ranges of scale and more realistic parameters, while observations achieve higher space and time resolution, for example in the Magnetosphere Multiscale, Solar Orbiter, and Solar Probe missions.

[1] R. Bruno and V. Carbone, Living Rev. Solar Phys. **2**, 4 (2005).

[2] E. Marsch, Living Rev. Solar Phys. **3**, 1 (2006).

[3] A. N. Kolmogorov, Dokl. Akad. Nauk SSSR **30**, 9 (1941).

[4] S. D. Bale, P. J. Kellogg, F. S. Mozer, T. S. Horbury, and H. Reme, Phys. Rev. Lett. **94**, 215002 (2005).

[5] O. Alexandrova, J. Saur, C. Lacombe, A. Mangeney, J. Mitchell, S. J. Schwartz, and P. Robert, Phys. Rev. Lett. **103**, 165003 (2009).

[6] F. Sahraoui, M. L. Goldstein, G. Belmont, P. Canu, and L. Rezeau, Phys. Rev. Lett. **105**, 131101 (2010).

[7] W. H. Matthaeus and D. Montgomery, Ann. N.Y. Acad. Sci. **357**, 203 (1980).

[8] D. Biskamp, Phys. Fluids **29**, 1520 (1986).

[9] V. Carbone, P. Veltri, and A. Mangeney, Phys. Fluids A **2**, 1487 (1990).

[10] J. Borovsky, J. Geophys. Res. **113**, A08110 (2008).

[11] L. F. Burlaga, Sol. Phys. **7**, 54 (1969).

[12] B. T. Tsurutani and E. J. Smith, J. Geophys. Res. **84**, 2773 (1979).

[13] B. J. Vasquez, V. I. Abramenko, D. K. Haggerty, and C. W. Smith, J. Geophys. Res. **112**, 11102 (2007).

[14] A. Greco, P. Chuychai, W. H. Matthaeus, S. Servidio, and P. Dmitruk, Geophys. Res. Lett. **35**, L19111 (2008).

[15] A. Greco, W. H. Matthaeus, S. Servidio, P. Chuychai, and P. Dmitruk, Astrophys. J. Lett. **691**, L111 (2009).

[16] S. Perri, M. L. Goldstein, J. C. Dorelli, and F. Sahraoui, Phys. Rev. Lett. **109**, 191101 (2012).

[17] H. Karimabadi, V. Roytershteyn, M. Wan, W. H. Matthaeus, W. Daughton, P. Wu, M. Shay, B. Loring, J. Borovsky, E. Leonardis, S. Chapman, and T. K. M. Nakamura [Phys. Plasmas (to be published)].

[18] K. T. Osman, W. H. Matthaeus, M. Wan, and A. F. Rappazzo, Phys. Rev. Lett. **108**, 261102 (2012).

[19] K. T. Osman, W. H. Matthaeus, B. Hnat, and S. C. Chapman, Phys. Rev. Lett. **108**, 261103 (2012).

[20] S. Servidio, F. Valentini, F. Califano, and P. Veltri, Phys. Rev. Lett. **108**, 045001 (2012).

[21] F. Valentini, P. Travnicek, F. Califano, P. Hellinger, and A. Mangeney, J. Comput. Phys. **225**, 753 (2007).

[22] F. Valentini, F. Califano, and P. Veltri, Phys. Rev. Lett. **104**, 205002 (2010).

[23] C. W Smith, K. Hamilton, B. J. Vasquez, and R. J. Leamon, Astrophys. J. **645**, L85 (2006).

[24] T. Hada, D. Koga, and E. Yamamoto, Space Sci. Rev. **107**, 463 (2003).

[25] R. Bruno, V. Carbone, P. Veltri, E. Pietropaolo, and B. Bavassano, Planet. Space Sci. **49**, 1201 (2001).

[26] P. Veltri and A. Mangeney, in "*Solar Wind IX*", AIP Conference Proceedings, Vol. 471, edited by S. Habbal (Nantucket, MA, USA, 1999), p. 543.

[27] A. Greco, W. H. Matthaeus, R. D'Amicis, S. Servidio, and P. Dmitruk, Astrophys. J. **749**, 105 (2012).

[28] K. T. Osman, W. H. Matthaeus, A. Greco, and S. Servidio, Astrophys. J. **727**, L11 (2011).

[29] S. Servidio, A. Greco, W. H. Matthaeus, K. T. Osman, and P. Dmitruk, J. Geophys. Res. **116**, A09102 (2011).